

THEORETICAL LIMB DARKENING FOR CLASSICAL CEPHEIDS. II. CORRECTIONS FOR THE GEOMETRIC BAADE-WESSELINK METHOD

MASSIMO MARENGO, MARGARITA KAROVSKA, DIMITAR D. SASSELOV, AND COSTAS PAPALIOLIOS¹
Harvard-Smithsonian Center for Astrophysics, 60 Garden Street, Cambridge, MA 02138; mmarengo@cfa.harvard.edu

JOHN T. ARMSTRONG
Remote Sensing Division, US Naval Research Laboratory, Code 7210, Washington, DC 20375

AND

TYLER E. NORDGREN
Department of Physics, University of Redlands, 1200 East Colton Avenue, Redlands, CA 92373
Received 2002 November 20; accepted 2003 February 10

ABSTRACT

The geometric Baade-Wesselink method is one of the most promising techniques for obtaining a better calibration of the Cepheid period-luminosity relation by means of interferometric measurements of accurate diameters. In this paper we present new wavelength- and phase-dependent limb-darkening (LD) corrections based on our time-dependent hydrodynamic models of the classical Cepheid ζ Gem. We show that a model simulation of a Cepheid atmosphere, taking into account the hydrodynamic effects associated with the pulsation, shows strong departures from the LD otherwise predicted by a static model. For most of its pulsational cycle the hydrodynamic model predicts a larger LD than the equivalent static model. The hydrodynamics affects the LD mainly at UV and optical wavelengths. Most of these effects evolve slowly as the star pulsates, but there are phases, associated with shocks propagating into the photosphere, in which significant changes in the LD take place on timescales of the order of less than a day. We assess the implication of our model LD corrections fitting the geometric Baade-Wesselink distance of ζ Gem for the available near-IR PTI data. We discuss the effects of our model LD on the best-fit result and analyze the requirements needed to test the time dependence of the LD with future interferometric measurements.

Subject headings: Cepheids — stars: atmospheres — stars: individual (ζ Geminorum) — stars: oscillations — techniques: interferometric

1. INTRODUCTION

With the recent advances in interferometry, the Baade-Wesselink (BW) method (Baade 1926; Wesselink 1946) has become one of the most promising techniques to obtain independent distance measurements of pulsating stars. A “geometric” variation of this classical method (Sasselov & Karovska 1994) can in principle be used to derive the distances of nearby classical Cepheids from the variations, as they pulsate, of their angular diameters and radial velocities. The potential accuracy of this method can improve the calibration of the period-luminosity relation of classical Cepheids (Leavitt 1908), which is a fundamental step in the cosmological distance ladder.

The geometric BW method has been recently applied to two Cepheids in the northern hemisphere, ζ Gem (Lane et al. 2000) and η Aql (Lane, Creech-Eakman, & Nordgren 2002). Both stars were observed at near-IR wavelengths (H band) with the Palomar Testbed Interferometer (PTI). The uniform-brightness disk diameter was measured at several epochs for both stars, with enough precision to detect the changes in the stellar radius due to the pulsation. The measured angular diameters were then fitted with an appropriate model derived from the radial velocities of the two stars, obtaining the distance with an estimated accuracy of $\sim 10\%$.

As explained in detail by Lane et al. (2002), the main source of uncertainty in the measurements is related to (1)

the conversion of photospheric line velocities into radial motion (the so-called projection factor, or p -factor) and (2) the estimate of the limb darkening (LD). These two quantities can be derived by modeling the Cepheid atmosphere, taking into account the spherical geometry of the star and the time-dependent hydrodynamics of the pulsations. The correct way to determine the p -factor for pulsating Cepheids has been described in detail in Sabbey et al. (1995) and Krockenberger, Sasselov, & Noyes (1997). More recently, we have presented a new method for computing accurate time- and wavelength-dependent center-to-limb brightness distributions for classical Cepheids (Marengo et al. 2002, hereafter Paper I).

The model described in Paper I provides a significant improvement of the LD coefficients with respect to the tabulated values currently used to analyze interferometric data. These tables (Parsons 1971; Manduca 1979; Kurucz 1993a; Claret, Díaz-Cordovés, & Giménez 1995) are based on hydrostatic model atmospheres of nonpulsating yellow supergiants, having T_{eff} and $\log g$ similar to those of classical Cepheids. Our models have the advantage of being specific for each simulated Cepheid, and they provide the appropriate LD for any pulsational phase at arbitrary wavelength. As shown in Paper I, the LD predicted by our models is significantly different from that expected for a static yellow supergiant.

In this paper we analyze how the inclusion of hydrodynamic effects in our Cepheid models can affect the interferometric distance determination with the geometric BW method. We first compute the LD corrections as a function

¹ We are saddened to report that our colleague, Costas Papaliolios, died 2002 June 6.

of wavelength and pulsational phase (§ 2), starting from the center-to-limb intensity profiles presented in Paper I for the classical Cepheid ζ Gem. Then we derive a new estimate for the geometric BW distance of this star, correcting the PTI data presented by Lane et al. (2002) with our phase- and wavelength-dependent LD corrections (§ 3). The accuracy of the best-fit values and the importance of various error sources are described in detail. We then conclude by analyzing the extent of the corrections induced by our models in the geometric BW distances and the level of accuracy that will be required by present and future interferometers to detect the hydrodynamic effects predicted by our models.

2. LIMB-DARKENING CORRECTIONS

The models described in Paper I consist of a series of synthetic atmospheres, computed with second-order, one-dimensional hydrodynamic calculations performed assuming a spherical symmetry. Each model simulates the atmosphere of a Cepheid at a certain pulsational phase. In Paper I we have described the general procedure to obtain such models and have shown the specific results for the classical Cepheid ζ Gem.

The pulsational period of ζ Gem (of approximately 10.15 days) was covered by a total of 49 individual models (the time step in our model grid is determined by the convergence criteria in the hydrodynamic simulation). The time resolution of our model sequence is thus ~ 0.2 days. For each model in the sequence, we have computed realistic spectral intensity distributions. This step was done by approximating the dynamic models with a plane-parallel atmosphere. The radiative transfer problem for the static atmosphere was then solved in LTE conditions using the ATLAS code (Kurucz 1970, 1979, 1993b) and its opacity library. The end result of this procedure is a set of 49 spectral intensity distributions describing the ζ Gem spectrum as it changes while the star pulsates.

In Paper I we showed how this procedure allows us to compute accurate LD profiles for ζ Gem that are (pulsational) phase- and wavelength-dependent. We proceed here to the next step, which is to describe how these models can be used in interferometry.

Interferometric measurements are usually expressed in terms of uniform-intensity disk (UD) or limb-darkened diameters. The UD diameters are derived by fitting the normalized fringe visibilities (squared) V^2 with a uniform-disk model, which assumes that the star is a disk of uniform brightness:

$$V_{\text{UD}}^2(\rho) = \left[\frac{2J_1(\pi\theta_{\text{UD}}\rho)}{\pi\theta_{\text{UD}}\rho} \right]^2, \quad (1)$$

where θ_{UD} is the UD angular diameter and ρ the spatial frequency of the measurement. Since a uniform-disk model is derived assuming that the source is a disk of uniform brightness, it does not depend on the wavelength. Real stars, however, are limb-darkened and have limb-to-center brightness distributions that are a function of wavelength, as shown in Paper I.

For any practical purpose, we can consider the physical radius of the stellar photosphere to be a well-defined quantity. The contribution functions of observable spectral features in the stellar spectra do peak at different heights in the atmosphere, but the difference is very small compared to the

full diameter of the star. For this reason, we can assume that the angular diameter of a Cepheid is the same at all wavelengths, after being corrected for LD. This diameter, which we call the “limb-darkened diameter,” $\theta_{\text{LD}}(\phi)$, since it takes into account the fact that the star has LD, will thus only depend on the pulsational phase of the star, and not on λ . Fitting fringe visibilities with a UD model, on the other hand, will produce a different θ_{UD} according to the wavelength, because of the inability of UD models to take into account the spectral properties of the LD. For this reason the UD angular diameter measured from fringe visibilities of a limb-darkened star will instead depend on both the pulsational phase and the wavelength: $\theta_{\text{UD}}(\lambda, \phi)$.

To obtain the real angular diameter of a star from the fringe visibilities, one can either fit the V^2 data with an appropriate LD model or correct the UD measurement with a specific, wavelength-dependent LD correction. The first approach is certainly preferable, because it preserves the wavelength dependence of the measured visibilities and thus allows a test of the LD models. There are cases, however, in which the original visibilities are not available, as, for example, when mixing heterogeneous data from different interferometers.

In this section we present accurate LD corrections derived using our models. They are based on hydrodynamic models, and therefore they are phase- and wavelength-dependent. Even though the models are specific for ζ Gem, we use them here as an example to describe the more general case of LD corrections for the generic classical Cepheids and their implications for interferometry and the BW method.

The conversion factor between UD and limb-darkened diameters is usually defined as $k(\lambda, \phi) = \theta_{\text{UD}}(\lambda, \phi)/\theta_{\text{LD}}(\phi)$. This factor is in many cases approximated by the model of a star having similar spectral type as the source of interest (in the case of Cepheids, a yellow supergiant, as described in Claret et al. 1995). Such approximations do not take into account the phase dependence for variable sources and may be incorrect in their dependence on λ , since the atmosphere of a Cepheid cannot be properly approximated with a static supergiant (see discussion in Paper I).

The $k(\lambda, \phi)$ corrections discussed in the following sections are derived with the following procedure. At each phase in the model grid, and for a set of wavelengths in the optical and near-IR range, the center-to-limb profiles computed in Paper I are converted into fringe visibilities by applying the Hankel transform (see, e.g., Koehler 1988):

$$V_{\text{LD}}^2(\rho, \phi) = \left[2 \int_0^\infty I_\nu(w, \lambda, \phi) J_0(w\rho) w dw \right]^2, \quad (2)$$

where ρ is the spatial frequency of the interferometric visibility, $w = (\theta_{\text{LD}}/2) \sin \alpha$ is the projection of the stellar angular radius on the disk, and $I_\nu(w, \lambda, \phi)$ is the model stellar intensity spectrum at the projected radius, computed for the given pulsational phase ϕ .

The simulated V_{LD}^2 visibilities are then fitted with a UD V_{UD}^2 model, in order to derive the UD diameter θ_{UD} , which the interferometer would have measured, at each wavelength, for the model source. The LD correction $k(\lambda, \phi)$ is the ratio between the best-fit θ_{UD} and the value of the angular diameter $\theta_{\text{LD}} = 1$ mas that we set to give a physical dimension to the simulated visibilities in the Hankel transform. The simulated visibilities were computed over a spatial frequency range up to the first minimum, to match the

typical conditions encountered when fitting real data with currently available interferometers. We have, however, tried several other combinations of model θ_{LD} and spatial frequency ranges (to simulate different interferometer base-lines), confirming that the resulting $k(\lambda, \phi)$ are not very sensitive to these parameters, as long as the simulated star is at least partially resolved.

2.1. Spectral Properties of LD

An example of the wavelength dependence of the LD correction $k(\lambda)$ is shown in Figure 1. The figure shows the LD correction derived from our hydrodynamic simulations (*thick line*). The thin line shows the LD correction obtained from hydrostatic atmospheres (Kurucz models) having the

$T_{\text{eff}}(\phi)$ and $\log g(\phi)$ measured as functions of the pulsational phase by Krockenberger et al. (1997). Note that the T_{eff} of the dynamic and static models, at each pulsational phase, is the same, since the observational effective temperature was used as an input parameter to compute the dynamic model. The $\log g$ is instead different in the two cases, as a consequence of the procedure followed to solve the radiative transfer in the hydrodynamic case and of the specific definition of the gravity terms in the hydrodynamic equations.

The k -correction is strictly related to the spectral properties of the source. The LD is higher (lower k) at UV and visible wavelengths and converges toward unity (no LD) with increasing wavelengths toward the infrared. Spectral lines

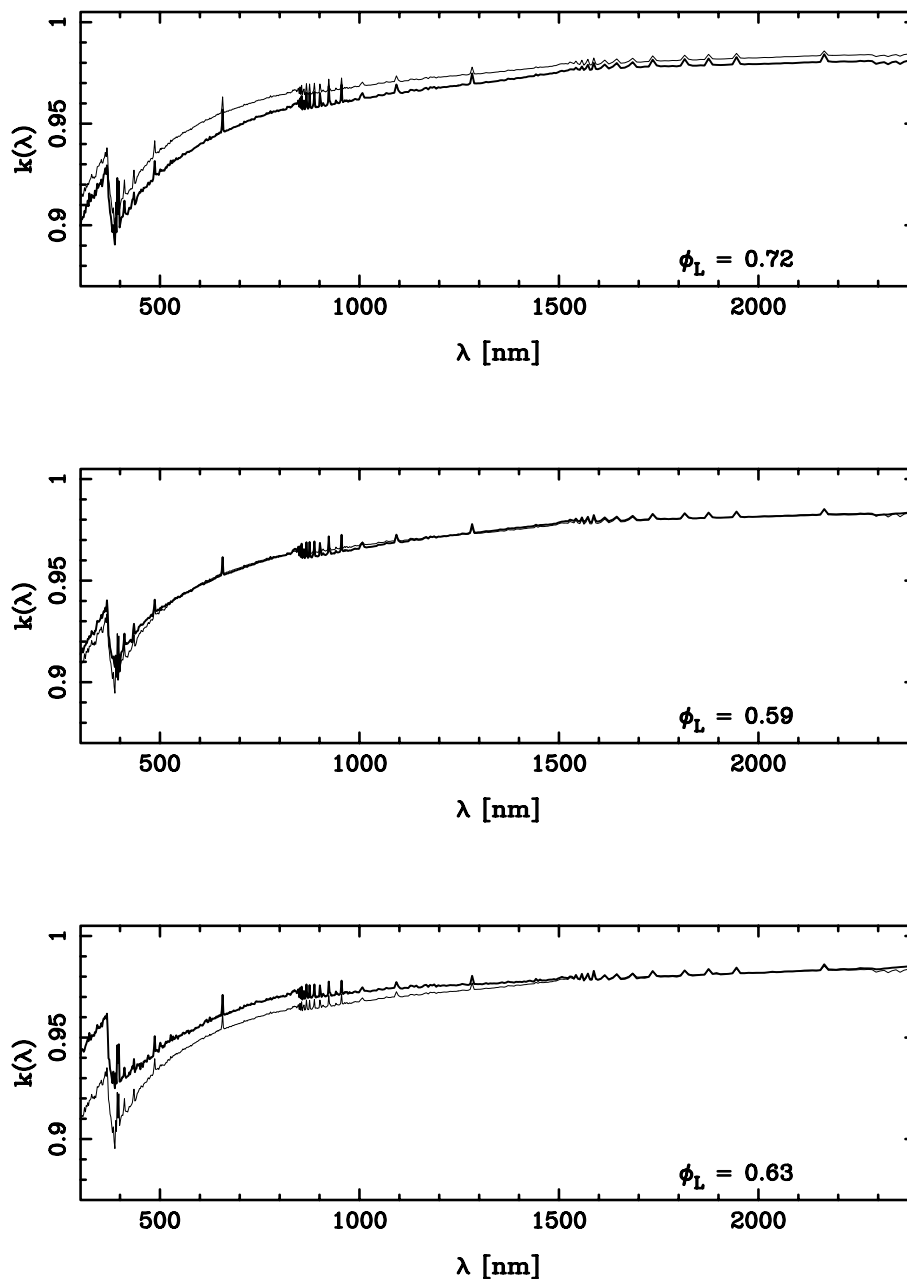


FIG. 1.—Wavelength dependence of the LD correction $k(\lambda)$ for our ζ Gem model. From top to bottom, the models are shown at minimum radius, at a quasi-static phase after maximum luminosity, and at the time in which a shock wave is crossing the atmosphere. The thick line is for $k(\lambda)$ from our hydrodynamic model, while the thin lines are derived from a hydrostatic model having T_{eff} and $\log g$ determined from observations (Krockenberger et al. 1997).

are less limb-darkened than the continuum: having higher optical depth, they probe upper atmospheric layers, where the temperature gradient is lower. Among the spectral features that are visible in our low spectral resolution computations are the Balmer jump in the UV, the Ca H and K doublet ($\lambda \simeq 395$ nm), H β ($\lambda \simeq 486$ nm), and H α ($\lambda \simeq 656$ nm).

The top panel in Figure 1 shows the LD correction at minimum radius. At this phase, the Cepheid atmosphere is most compressed, giving rise to a steeper temperature gradient. This is responsible for an increase of the LD at all wavelengths. The LD correction for the hydrostatic atmosphere, on the other hand, does not show this same effect, having a flatter LD despite the fact that T_{eff} is the same in the two models. The difference is as much as $\Delta k \simeq 0.01$ at visible wavelengths and less in the near-IR. Accurate measurements of the LD with optical interferometers should then be able to verify this effect. The difference between the static and dynamic models is even larger at the wavelengths of the main spectral features, which appear stronger in the more compressed hydrodynamic atmosphere.

In the next section, we show that in most cases the effects of the hydrodynamics on the atmospheric structure result in a larger LD. There are, however, phases in which the free expansion of the atmosphere results in a *quasi-static* structure. In these phases (before and after maximum luminosity), the hydrodynamics is less important and the two $k(\lambda)$ are virtually indistinguishable.

As shown in the bottom panel of Figure 1, however, the full force of a shock wave crossing the photosphere results in high excitation states and local expansion. Even though at this phase ζ Gem is contracting (this happens 1 day before minimum radius), the energy deposited by the shock in the region where the visible photons are created generates a lower temperature gradient. As a consequence, the LD of the hydrodynamic simulation is lower than in the static case. Note, however, that this effect is mostly appreciable at visible wavelengths. An optical interferometer should detect at this phase a decrease of the LD of $\Delta k \simeq 0.01$. This phase is very brief and, at least in the case of ζ Gem, the effects of the shock are already dissipated after less than 20 hr, when the LD is maximum again as the star approaches minimum radius. This timescale is related to the shock propagation speed, which is very well constrained by observations (see Fig. 8 of Sasselov & Lester 1994).

2.2. LD and Pulsational Phase

By convolving the $k(\lambda, \phi)$ models with the filter passbands used by interferometers, we can study the variations of the LD correction as a function of the pulsational phase. For a convenient comparison with observations, the best choice is to adopt the phase as defined by the optical light curve, where the zero phase, $\phi_L = 0$, coincides with maximum luminosity. As explained in Paper I, however, our dynamic simulations are computed as a function of the phase ϕ_V based on the pulsational velocity, in which the zero phase is at minimum radius. To convert our LD models to the light-curve phases, we have used the phase shift $\Delta\phi = \phi_L - \phi_V$ between maximum luminosity and minimum radius computed by Bersier, Burki, & Burnet (1994a) and Bersier et al. (1994b).

Figure 2 shows the LD corrections plotted as a function of the visible light-curve phase for two wavelengths. The

top panel shows $k(\phi)$ for the near-IR H -filter passband used by the PTI interferometer. The bottom panel shows $k(\phi)$ for the bluest available channel ($\lambda \simeq 570$ nm) of the Navy Prototype Optical Interferometer (NPOI) in the optical. The curves have been filtered to remove numerical noise with an adaptive Gaussian kernel, and the rms error bands in our LD corrections associated with the numerical uncertainty are indicated by two thin lines bracketing each LD curve.

The plots show that $k(\phi)$ is roughly constant for most phases, with a slow increase as the star expands, as a consequence of the decreasing temperature gradient in the photosphere. Coincident with the passage of a shock wave through the photosphere (at $\phi_L \simeq 0.6$), $k(\phi)$ shows a sudden rise in the optical, indicative of a sharp decrease in the LD. The energy deposited by the shock is responsible for this effect. It increases the excitation in the photospheric layers and thus flattens the temperature gradient. This extra energy dissipates in a short timescale, after which the atmosphere resumes its normal state. At $\phi_L \simeq 0.7$ ζ Gem is close to minimum radius, where the temperature gradient is higher (because of the compression of the atmosphere), and thus the star appears more limb-darkened.

The sharp increase in $k(\phi)$ observed in the optical at the time of the shock wave is not predicted for the H band. This is because in this wavelength range the effects of the shock

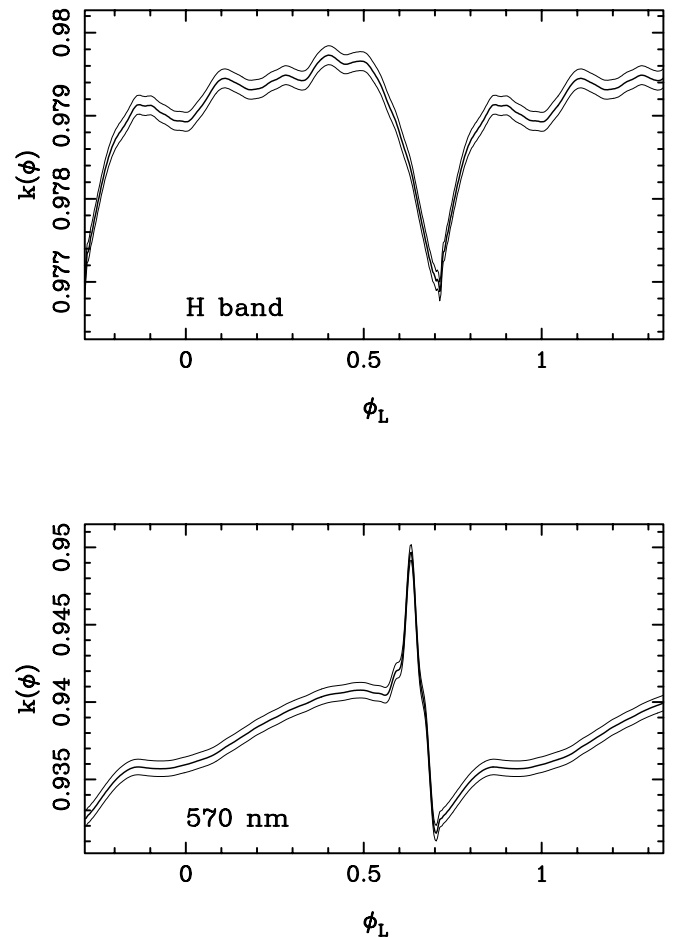


FIG. 2.—Pulsational phase dependence of the LD correction $k(\phi)$ for our ζ Gem model. The LD correction is shown for the near-IR H band (top) and at visible wavelength (570 nm; bottom). The thin lines show the rms numerical uncertainties in our simulations.

are less pronounced. This might be due to the fact that the emergent spectrum in the H band originates deepest in the atmosphere, as a result of the broad minimum of the H^- opacity at $1.6 \mu\text{m}$, and the shocks increasingly steepen and disturb the atmosphere as they propagate down the density gradient (up into the atmosphere).

It is important to understand how much of this behavior in the LD curves is due to hydrodynamic effects or just to the changes in T_{eff} and $\log g$ during the stellar pulsation. Solid lines in Figure 3 show our hydrodynamic simulations for two wavelengths. The dotted lines show the LD correction derived for hydrostatic atmospheres having at each phase the T_{eff} and $\log g$ measured by Krockenberger et al. (1997), which we used as starting points in our models. The overall value of $k(\phi)$ is similar, at each wavelength, in the hydrodynamic and hydrostatic atmospheres. The phase dependence is instead completely different. Figure 4 reveals that static model LD corrections closely follow the change of T_{eff} with phase. In a hydrostatic atmosphere, a higher T_{eff} is responsible for a flatter photospheric temperature gradient and thus for less LD (i.e., higher k). In a hydrodynamic atmosphere the temperature gradient is determined predominantly by the pulsation dynamics, and

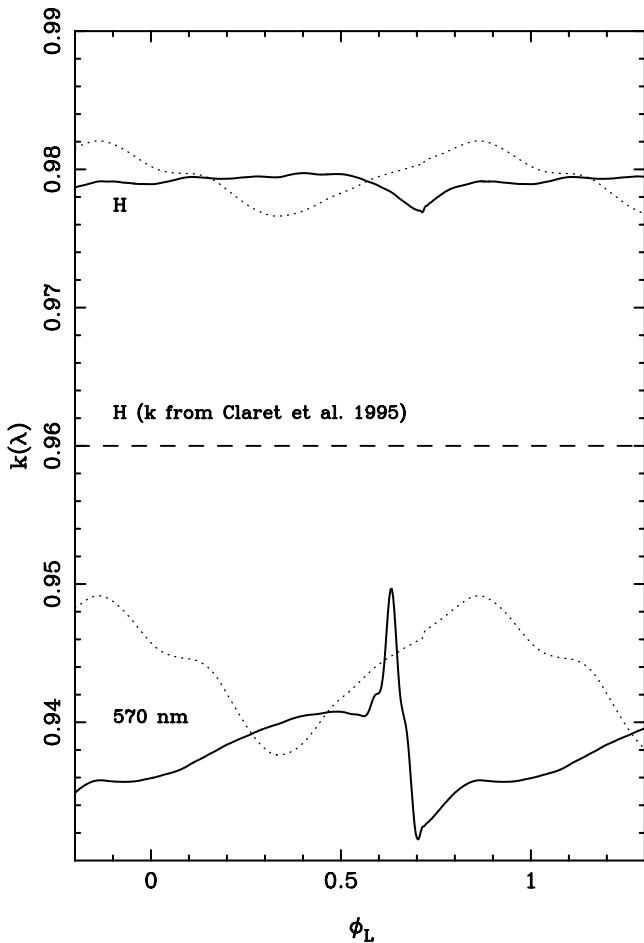


FIG. 3.—Phase-dependent $k(\phi_L)$ for ζ Gem in the PTI H band and in the bluest 570 nm channel of the NPOI. Solid lines show the LD corrections computed with our hydrodynamic model; dotted lines show the equivalent corrections for a hydrostatic atmosphere having T_{eff} and $\log g$ from Krockenberger et al. (1997). The dashed line shows the value computed by Claret et al. (1995) and used in Lane et al. (2002).

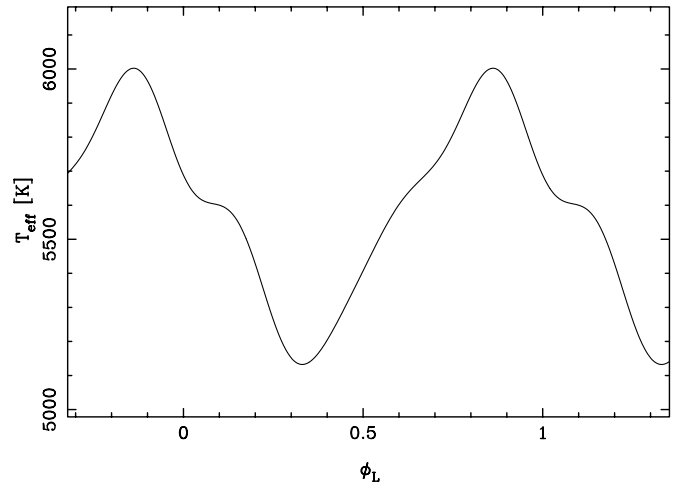


FIG. 4.—Effective temperature as a function of light-curve phase, used to compute the hydrodynamic model of ζ Gem. The dependence of T_{eff} on the pulsational phase is derived from measurements by Krockenberger et al. (1997).

therefore the phase dependence of the LD is different. In a hydrostatic atmosphere, gravity seems to have little or no effect in determining the changes in the LD. When computing the spectral energy distribution of our dynamic atmosphere, we constrain the model T_{eff} to the observed values, leaving $\log g$ as a free parameter to be fitted with a grid of static atmospheres (see Paper I). The rationale for this choice was that T_{eff} has a dominant role in determining the spectral properties of the atmosphere. This result confirms the validity of our choice.

To test the assumption that $\log g$ does play a minor role, we have also computed the LD correction for the static models having *both* T_{eff} and $\log g$ identical to the hydrodynamic simulations. The results are very similar. Despite the significantly different $\log g$ with respect to the observed values, $k(\phi)$ still closely follows the variations of T_{eff} . Only just after minimum radius (when T_{eff} is maximum and the best-fit $\log g$ is minimum), $\log g$ plays some role in lowering the LD correction. This confirms that, except when $\log g$ is very small (~ 1 , in this case), the effective temperature is the decisive parameter for the LD in a hydrostatic atmosphere.

In a hydrodynamic atmosphere, however, T_{eff} is *not* the dominant parameter. As shown in Figure 3, when hydrodynamic effects are taken into account, the relation between T_{eff} and the LD breaks. Shocks are the source of the most dramatic effects in $k(\phi)$, but even when they are absent, the LD corrections are strikingly different from the ones predicted by hydrostatic atmospheres. This is because they are determined not by T_{eff} , but by the time-dependent structure of the expanding/contracting atmosphere. Given that our hydrodynamic models generally have a steeper temperature gradient than a similar hydrostatic atmosphere, the resulting LD is larger for most phases.

Figure 3 also shows the LD correction used in Lane et al. (2002) for ζ Gem, which has the constant value of $k = 0.96 \pm 0.01$. This correction has been derived from tables published by Claret et al. (1995), based on hydrostatic models. Note that the average value of our LD correction is outside the error bars of the tabulated value. The reason for this discrepancy is that our model closely follows the T_{eff} and $\log g$ derived for ζ Gem from spectroscopic

observations, while the Claret et al. (1995) values are computed for a generic grid of yellow supergiants matching the Cepheid's spectral type.

Note finally that, as expected, the LD correction is much smaller at near-IR wavelengths and larger toward the blue. At bluer wavelengths the amplitude of the k -variations with phase (especially at the time of the shock wave) is also much larger. Therefore, to test observationally the details of the hydrodynamic effects on LD, interferometers operating at short wavelengths are favored.

3. EFFECTS OF THE LD CORRECTIONS ON THE GEOMETRIC BW METHOD

The LD deviations introduced by the hydrodynamics are relatively small (1% in the optical and less in the infrared) and are thus usually ignored when treating interferometric measurements. In order to obtain accurate distances with the BW geometric method, however, higher levels of accuracy are needed. Under such stringent requirements, the time- and wavelength-dependent hydrodynamic effects play an important role and should be taken into account.

A detailed description of the problems involved with the application of the geometric BW method to pulsating Cepheids is given in Sasselov & Karovska (1994). This method allows the determination of the distance and the average radius of a pulsating star from both its angular diameter and radial velocity at several phases. This is done by means of a χ^2 fit of the function

$$\chi^2 = \sum_i \left\{ \frac{[\Theta_0 + (2\Delta R_i/D)] - \theta_i}{\sigma_i} \right\}^2, \quad (3)$$

where $\Theta_0 = 2R_0/D$ is the average angular radius of the star and ΔR_i its radial displacement at the time of the interferometric measurement θ_i . The variation of the stellar radius $\Delta R(\phi_L)$ is derived, as a function of the light-curve phase ϕ_L , by integrating the pulsational velocity over time:

$$\Delta R(\phi_L) = - \int_{\phi_0}^{\phi_L} p[v_r(\phi') - \gamma] d\phi', \quad (4)$$

where $v_r(\phi)$ is the radial velocity, which is corrected by the systemic velocity γ and the p -factor to yield the true pulsational velocity. The systemic velocity can be derived by requiring the conservation of the radius over one period (see Paper I). Appropriate p -factors have been computed for pulsating Cepheids, such as ζ Gem; we use here the value of 1.43 (the same adopted by Lane et al. 2002), derived from the hydrodynamic model we used to compute our LD profiles, which was published in Sabbey et al. (1995).

The fit in equation (3) can be solved analytically. The best-fit R_0 and D can be derived by minimizing the χ^2 relation, solving for the two unknown parameters. Note that we do not make use of the color curve of the Cepheid, which can be applied to further constrain the geometric BW solution. A detailed description of this procedure will be given in a separate paper.

The LD corrections $k(\phi)$ computed in the previous sections enter the fit by allowing the conversion of the UD diameters $\theta_{UD}^{(i)}$ obtained by the interferometer into true limb-darkened diameters of the star: $\theta_i = \theta_{UD}^{(i)}/k(\phi_i)$, where $k(\phi_i)$ is the LD correction at the phase of the i th measurement, computed for the wavelength of the observation.

TABLE 1
BW BEST FIT OF ζ GEM PTI H -BAND LD DATA

Fit Parameter (1)	$k(\phi)$ (model) (2)	$k = 0.96$ (3)
$R_0 (R_\odot)$	$67.0^{+8.7}_{-6.9}$	$66.2^{+8.3}_{-6.6}$
D (pc).....	372^{+49}_{-39}	361^{+46}_{-36}
Θ_0 (mas).....	1.665 ± 0.007	1.698 ± 0.007
χ^2	28.1	29.5

The terms σ_i in the fit χ^2 relation are the errors associated with each data point. They are the geometric sum of the individual error sources (in terms of angular diameters) for each observation:

$$\sigma_i^2 = \left(\sigma_i^{(\theta)} \right)^2 + \left(\sigma_i^{(\Delta R/D)} \right)^2 + \left(\sigma_i^{(k)} \right)^2, \quad (5)$$

where $\sigma_i^{(\theta)}$ is the error of the interferometric measurements, $\sigma_i^{(\Delta R/D)}$ the error related to the radial displacement, and $\sigma_i^{(k)}$ the error in the LD correction. According to Lane et al. (2002), the errors in the PTI H -band data vary between 0.01 and 0.06 mas. The errors on the radial displacements are due to the uncertainty in the p -factor (amounting to $\sim 4\%$, according to Sabbey et al. 1995), and to the estimated measurement errors in the radial velocity, adding a further 2% according to Bersier et al. (1994b). The errors in our LD corrections, barring systematic errors and based only on the numeric uncertainty in our model, are of the order of $\pm 0.02\%$ (see Fig. 2), which is a negligible contribution with respect to the other error sources, and it is thus ignored.

The best-fit results are shown in Table 1 (col. [2]) and Figure 5. Column (3) in Table 1 shows, for comparison, the best-fit parameters obtained with the same fixed LD correction used by Lane et al. (2002) of $k \simeq 0.96$. The difference in the two best-fit values of the geometric BW distance is 11 pc,

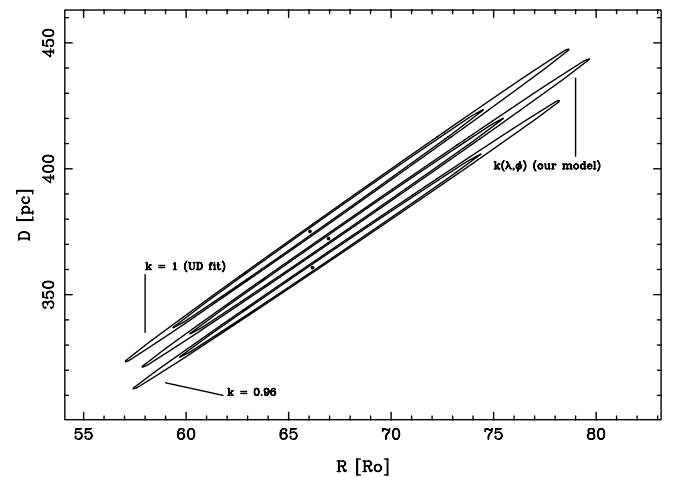


FIG. 5.—Best-fit parameters and error regions for ζ Gem PTI H -band data. The top curve is for the UD data, the middle curve is for our best fit for model LD data, and the bottom curve is for the result obtained using a fixed LD correction of $k \simeq 0.96$, as in Lane et al. (2002). The inner error region is the 68% confidence level of the fit (1σ), while the outer is the 90% confidence level.

which is less than $\sim 3\%$. Even though this difference is less than $\frac{1}{3}$ of the error bars, it is significant: Figure 5 shows that the error regions for our best fit, the UD fit, and the fixed- k fit are mutually exclusive. This is again a consequence of the high level of precision that the available interferometric data already allow in the determination of the average angular radius Θ_0 .

Note that the error regions shown in Figure 5 do not take into account the uncertainty in the LD correction, which we ignored. The uncertainty quoted for the tabulated LD correction used by Lane et al. (2002) is much larger than our numeric error, $\Delta k \simeq 0.02$, and would have resulted in a much larger error region, including all the narrow ovals in Figure 5. The main point of this paper, however, is to discuss the consequences of using model-derived LD corrections, and Figure 5 shows that in the case of ζ Gem using generic tabulated LD corrections can lead to an error of a few percent with respect to the best-fit distance. This discrepancy is larger than the error regions determined by all the other error sources and can thus in principle be tested observationally by directly measuring the LD with longer baseline interferometers.

The differences in the results of the geometric BW fit are entirely due to the LD correction, more precisely to its *average value* \bar{k} computed over the pulsational cycle. In the near-IR, and especially in the H band, the phase dependence of $k(\lambda, \phi)$ is relatively small (less than 2%, compared with the error bars $\gtrsim 5\%$ – 10% in the measured angular diameters). This means that, with the current error bars in the interferometric data, we are still not sensitive to the variations in the LD corrections induced by the hydrodynamics. An accuracy of the order of 0.2% in the θ_i is required to be sensitive to such effects in the H band. Note that a more favorable situation is met in the visible, where the temporal variations of $k(\phi)$ are larger. Given the limitation of the available data, however, the main contribution of our hydrodynamic simulations, at least for now, is not in the detailed dependence of $k(\phi)$, but in setting the right level of the LD correction for the wavelength of the observation. Contrary to the tabulated values of the LD correction, which are computed for generic yellow supergiants having the same spectral type as Cepheid stars, our corrections are specific for the modeled stars, as they follow the T_{eff} and $\log g$ derived from spectroscopic observations for each star. This is not a trivial matter, as the discrepancy with the tabulated value ($\Delta k \simeq 0.02$ in the H band) is the largest error source in the determination of the geometric BW distance.

Finally, we discuss the issue of the validity of the best-fit χ^2 as a guide to which LD better represents the data. Is the best-fit χ^2 an indicator of the best value for the LD correction? If this is the case, then we should conclude that ζ Gem is not limb-darkened, since the best-fit χ^2 computed with this same procedure with the UD diameters would be $\chi^2 \simeq 27.5$. However, this is not the case.

To explain this, one should first remember that the time-dependent hydrodynamic effects are too small to be observed with the available PTI data. While doing the BW fit, we could thus consider the LD correction as a constant value \bar{k} equal to its average over the pulsational period. In the three fits shown in Figure 5, the value of \bar{k} would be equal to 1 for the UD data, ~ 0.979 for our hydrodynamic calculations, and 0.96 for Claret et al. (1995; used by Lane et al. 2002). This coefficient enters the χ^2 equation by dividing

the UD $\theta_{\text{UD}}^{(i)}$:

$$\chi^2 = \sum_i \left\{ \frac{[\Theta_0 + (2\Delta R_i/D)] - (\theta_{\text{UD}}^{(i)}/\bar{k})}{\sigma_i} \right\}^2. \quad (6)$$

A smaller value of \bar{k} (larger LD), will result in a larger best-fit mean angular diameter Θ_0 , which will thus scale as $1/\bar{k}$. The net effect of this scaling is that the best-fit χ^2 will scale as $1/\bar{k}$. This means that a fit made with larger LD (as long as the phase dependence of k is irrelevant) will have a larger best-fit χ^2 . The UD fit will thus appear always to be the best.

The conclusion is that, until the accuracy of the measured angular diameters becomes good enough to appreciate the changes in LD due to the pulsation, the geometric BW fit is not a good tool to test the LD models. On the other hand, a good model for the LD is absolutely necessary to obtain a reliable value of the geometric BW distance, since the best-fit angular diameter scales linearly as $1/\bar{k}$.

Note, finally, that a different fitting strategy may allow a test of our LD models even with present-day interferometric data. Our insensitivity to the LD is due to the fact that we are fitting derived data (the angular diameters θ_i) that have been previously obtained from the fringe visibilities *assuming* a uniform-disk model. This initial fit has destroyed the sensitivity of the original data to the stellar LD. The correct way to test the LD is to perform χ^2 fits on the original visibilities. Any test for the absolute value of LD predicted by our models should thus be made using the visibility data taken at different projected baselines and wavelengths.

4. CONCLUSIONS

The geometric BW method is a powerful tool to derive the distances of pulsating stars. The detailed analysis of the method and our discussion of its main current uncertainties, described in the previous sections, show that special care should be taken when assessing the accuracy of the results.

Despite the increasing quality of the interferometric data, the error bars in the individual measurements are the largest contributors to the final errors in the geometric BW distances and average radii. After the instrumental errors, however, follows the uncertainty in the LD correction. The importance of LD will grow in the near future, given the fast pace at which the available interferometers are improving their accuracy, and with the new long-baseline, large-aperture interferometers that are becoming operational. To address this issue, we have presented in this paper a procedure to compute accurate LD corrections for pulsating Cepheids that are based on time- and wavelength-dependent hydrodynamic models.

We show that our $k(\lambda, \phi)$ strongly differ from the equivalent corrections computed from hydrostatic atmospheres, even in the absence of “strong” hydrodynamic effects like shocks. The main consequence of the hydrodynamic terms in our stellar atmospheric models is an increase in the LD because of a generally higher temperature gradient in the photosphere. The situation briefly reverses in presence of shock waves, because of the energy deposited by the shocks.

The magnitude of these effects depends on the wavelength. The effect is more significant in the visible spectrum ($\Delta k \sim 0.015$), and it is smaller in the infrared ($\Delta k \sim 0.002$). Current interferometers still cannot test these time-dependent variations in the LD, which will, however,

become important in the near future, especially when interferometric observations in spectral lines will become feasible. The phases of rapid variation in the LD associated with the propagation of the shock wave in the photosphere, when significant changes in the LD occur on timescales of hours, appears particularly appealing for an observational test of our models.

Even though the time-dependent variations in the LD are not currently measurable because of the required accuracy, our models can already provide an average value of the wavelength-dependent LD correction, $k(\lambda)$, that is significantly different from the tabulated values currently used. In the case of ζ Gem, our LD corrections induce a $\sim 3\%$ change in the best-fit value of the BW distance derived from H -band PTI data. Even more important is that, as shown in § 3, the 1σ error regions around the best-fit distances derived with our and other LD corrections are mutually exclusive, opening the possibility of an independent test of our models when longer baselines reaching the first minimum in the visibilities will allow a direct test. A preliminary test of our models will also be possible by directly fitting the observed

visibilities with our model visibilities, instead of using LD corrections of UD best-fit diameters.

As the data for other Cepheids become available, it will be important to have a large library of models specifically computed for each source. As the models are very dependent on the pulsational characteristics of each star, on which the hydrodynamic model is built, a “generic” parametric LD correction for all stars is not possible, as any individual model cannot be extended to be used for a Cepheid with a different pulsational engine. This is the reason why tables of LD corrections, such as the ones produced by Claret et al. (1995), cannot reproduce the detailed changes in the LD that are required to apply the geometric BW method to classical Cepheids.

We wish to thank the anonymous referee and the editor for the comments and suggestions that helped us to improve this paper. This work was partially supported by NFS grant AST 98-76734. M. K. is a member of the *Chandra* Science Center, which is operated under contract NAS 8-39073 and is partially supported by NASA.

REFERENCES

- Baade, W. 1926, *Astron. Nachr.*, 228, 359
 Bersier, D., Burki, G., & Burnet, M. 1994a, *A&AS*, 108, 9
 Bersier, D., Burki, G., Mayor, M., & Duquennoy, A. 1994b, *A&AS*, 108, 25
 Claret, A., Díaz-Cordovés, J., & Giménez, A. 1995, *A&AS*, 114, 247
 Koechlin, L. 1988, in *Proc. NOAO-ESO Conference on High-Resolution Imaging by Interferometry*, ed. F. Merkle (Garching: ESO), 715
 Krockenberger, M., Sasselov, D. D., & Noyes, R. W. 1997, *ApJ*, 479, 875
 Kurucz, R. L. 1970, *SAO Spec. Rep.* 309
 ———. 1979, *ApJS*, 40, 1
 ———. 1993a, in *Light-Curve Modeling of Eclipsing Binary Stars*, ed. E. F. Milone (New York: Springer), 93
 ———. 1993b, CD-ROM 13, *ATLAS9 Stellar Atmosphere Programs and 2 km/s Grid* (Cambridge: SAO)
- Lane, B. F., Creech-Eakman, M. J., & Nordgren, T. E. 2002, *ApJ*, 573, 330
 Lane, B. F., Kuchner, N. J., Boden, A. F., Creech-Eakman, M., & Kulkarni, S. R. 2000, *Nature*, 407, 485
 Leavitt, H. S. 1908, *Ann. Astron. Obs. Harvard Coll.*, 60, 87
 Manduca, A. 1979, *A&AS*, 36, 411
 Marengo, M., Sasselov, D. D., Karovska, M., Papaliolios, C., & Armstrong, J. T. 2002, *ApJ*, 567, 1131 (Paper I)
 Parsons, S. B. 1971, *ApJ*, 164, 355
 Sabbey, C. N., Sasselov, D. D., Fieldus, M. S., Lester, J. B., Venn, K. A., & Butler, R. P. 1995, *ApJ*, 446, 250
 Sasselov, D. D., & Karovska, M. 1994, *ApJ*, 432, 367
 Sasselov, D. D., & Lester, J. B. 1994, *ApJ*, 423, 777
 Wesselink, A. 1946, *Bull. Astron. Inst. Netherlands*, 10, 91